

Research paper

# Visibility graph analysis for re-sampled time series from auto-regressive stochastic processes

Rong Zhang<sup>a</sup>, Yong Zou<sup>a,\*</sup>, Jie Zhou<sup>a</sup>, Zhong-Ke Gao<sup>b</sup>, Shuguang Guan<sup>a</sup><sup>a</sup>Department of Physics, East China Normal University, 200062 Shanghai, China<sup>b</sup>School of Electrical Engineering and Automation, Tianjin University, 300072 Tianjin, China

## ARTICLE INFO

## Article history:

Received 8 January 2016

Accepted 25 April 2016

Available online 8 June 2016

## Keywords:

Visibility graph

AR processes

Nonlinear time series analysis

## ABSTRACT

Visibility graph (VG) and horizontal visibility graph (HVG) play a crucial role in modern complex network approaches to nonlinear time series analysis. However, depending on the underlying dynamic processes, it remains to characterize the exponents of presumably exponential degree distributions. It has been recently conjectured that there is a critical value of exponent  $\lambda_c = \ln 3/2$ , which separates chaotic from correlated stochastic processes. Here, we systematically apply (H)VG analysis to time series from autoregressive (AR) models, which confirms the hypothesis that an increased correlation length results in larger values of  $\lambda > \lambda_c$ . On the other hand, we numerically find a regime of negatively correlated process increments where  $\lambda < \lambda_c$ , which is in contrast to this hypothesis. Furthermore, by constructing graphs based on re-sampled time series, we find that network measures show non-trivial dependencies on the autocorrelation functions of the processes. We propose to choose the decorrelation time as the maximal re-sampling delay for the algorithm. Our results are detailed for time series from AR(1) and AR(2) processes.

© 2016 Elsevier B.V. All rights reserved.

## 1. Introduction

In the last years, complex network representations of time series have been proposed to characterize the underlying system [1–6], covering a great variety of fields of applications. For example, recurrence network approaches have been applied to climate data analysis [4,7], chaotic electro-chemical oscillators [8], or two-phase flow data [9]. Some basic network motif structures have been identified in music data [10]. Visibility graph (VG) and horizontal visibility graph (HVG) algorithms have been successfully applied to hurricane data in the US [11], financial market [12], turbulence [13,14], and sunspot time series [15,16], providing novel insights from a complex systems perspective. Several other methods have been discussed in [10]. In this work, we construct (H)VGs [3,17,18] for time series generated by auto-regressive models.

To apply (H)VG approaches, a proper transformation of the time series to a network representation is required. The VG algorithm maps a time-ordered set of  $N$  real numbers to a graph  $G$  with  $N$  nodes, which is completely described by the binary  $N \times N$  adjacency matrix  $\mathbf{A}$ . More specifically, let us consider a univariate time series  $\mathbf{x} = [x_1, x_2, \dots, x_i, \dots, x_N]$ , where  $N$  denotes the time series length and the subscript  $i$  represents the discrete sampling time. In terms of the associated VG, individual observations are interpreted as vertices of a complex network, and edges are placed between pairs of vertices

\* Corresponding author.

E-mail address: [yzou@phy.ecnu.edu.cn](mailto:yzou@phy.ecnu.edu.cn) (Y. Zou).

that exhibit some visibility condition, namely,

$$\frac{x_i - x_k}{k - i} > \frac{x_i - x_j}{j - i}, \tag{1}$$

which has to be fulfilled for all time points  $k$  with  $i < k < j$  [3].

As a notable modification of the VG algorithm, the simplified HVG criterion has been proposed in [17]. Specifically, two observations made at times  $i$  and  $j$  are considered to be connected in a HVG if and only if

$$x_k < \min(x_i, x_j) \tag{2}$$

for all  $k$  with  $i < k < j$ . It can be easily seen that the edge set of the HVG associated with a given time series is a subset of the edge set of the associated VG. One advantage of the HVG is that for certain simple stochastic processes, some basic graph properties can be calculated analytically [18].

Recent work on (H)VGs has mainly concentrated on the properties of the degree distribution  $p(k)$ . Concerning the HVG, exponential functional forms have been obtained for many random processes, namely,  $p(k) \sim e^{-\lambda k}$ . A scaling factor of  $\lambda_c = \ln(3/2)$  has been found in the case of uncorrelated noise (white noise), which has been further proposed to separate stochastic from chaotic dynamics in the following senses [18–20]: (i) correlated stochastic series are characterized by  $\lambda > \lambda_c$ , slowly tending to an asymptotic value of  $\ln(3/2)$  for very weak correlations, whereas (ii) chaotic series are often characterized by  $\lambda_{chaos} < \lambda_c$  for decreasing correlations or increasing chaos dimensionality, respectively [18]. In this work, we provide some further examples supporting argument (i). Meanwhile, we show some peculiar results indicating that  $\lambda_c$  should not be interpreted as a general critical value separating chaos from noise.

In fractal processes, numerical results suggest that  $p(k)$  exhibits a power law [3],  $p(k) \sim k^{-\gamma}$ . For instance, VG analysis has been suggested to characterize fractional Brownian motions, finding some heuristic relationship between  $\gamma$  and the process' Hurst exponent [21,22]. Depending on the fractality properties of the underlying process, recently an algorithm for constructing VGs from segmented time series has been proposed [23], which estimates power-law exponents reflecting scale-free properties quite well. The idea hinges on a proper choice of the time delay  $\tau$ , which re-samples the original time series resulting in a number of segmentations. As we will discuss below, the number of segments to be used is often not known in the original algorithm. In other words, we do not know the upper bound of  $\tau_{max}$  to terminate the computation. So far, only a heuristic choice of  $\tau_{max}$  has been suggested when network characteristics of segmented time series show more or less convergent behavior [23].

In this work, we will focus on applying (H)VG analysis to auto-regressive (AR) stochastic processes, which often describe certain time-varying processes in nature, economics, etc. AR models also have wide applications to climate research. The AR model specifies that the output variable depends linearly on its own previous values and on a stochastic term. More specifically,  $\mathbf{x} = [x_1, x_2, \dots, x_i, \dots, i \in \mathbb{Z}]$  is an AR model of order  $p$  denoted as AR( $p$ ) if

$$x_t = \sum_{j=1}^p \varphi_j x_{t-j} + \varepsilon_t, \tag{3}$$

where  $\varphi_j, j \in [1, p]$ , are real-valued coefficients of the model, and  $\varepsilon_t$  is white noise. We further assume that the error terms  $\varepsilon_t$  follow a Gaussian distribution with zero mean and unit variance. Specifically, we will perform both VG and HVG analysis for AR(1) and AR(2) processes in their stationary regimes, namely, (i)  $|\varphi_1| < 1$  for the AR(1) model, and (ii)  $\varphi_1 + \varphi_2 < 1, \varphi_2 - \varphi_1 < 1, |\varphi_2| < 1$  for the AR(2) model. Time series of AR models exhibit serial correlations conveniently captured by the autocorrelation function (ACF). For AR( $p$ ) processes, the ACFs can be computed analytically [24]. In general, the correlation length of a stochastic process increases if the corresponding ACF shows rather slow decays to zero [25].

The objectives of this work are the following. First, we test the hypothesis of the universality of the critical value of  $\lambda_c$  when anti-correlated increments are present in AR processes. Second, we apply the re-sampling algorithm to time series from AR( $p$ ) models and extend the existing (H)VG analysis from disclosing degree distribution properties to characterizing global network properties. Third, we suggest to choose the decorrelation time of the given time series as the maximal delay  $\tau_{max}$  for the re-sampling algorithm, after which network measures converge to some asymptotic values that are expected for uncorrelated stochastic processes with the given probability distribution function.

This paper is organized as follows: In Section 2, we review the main network measures that will be used in this work. We present the re-sampling algorithm to obtain segmented time series in Section 3. The results will be shown in Section 4 and some conclusions are drawn in Section 5.

## 2. Structural properties of (H)VG

We characterize the structural properties of VG and HVG based on the following two aspects: (i) degree distributions  $p(k)$  and (ii) global network measures.

### 2.1. Degree distributions

The degree  $k_i$  of a node  $i$  simply counts the number of direct connections associated with  $i$ ,  $k_i = \sum_j A_{i,j}$ , where  $A$  is the adjacency matrix. The degree distribution  $p(k)$  gives the fraction of nodes in the network with degree  $k$ . Exponential

functional forms have been reported for many stochastic processes,  $p(k) \sim e^{-\lambda k}$ . When estimating the scaling parameter  $\lambda$ , it is often useful to employ the cumulative probability distribution  $F(k) = \sum_{k>k_0} p(k)$  to obtain a more robust statistical fitting [26].

## 2.2. Global network measures

Many quantitative measures have been proposed in the literature to characterize networks, making use of local, meso-scale and global structural information [27]. Here, we focus on the following network measures:

- (i) *Network transitivity*  $\mathcal{T}$  [27,28], which globally characterizes the linkage relationships among triples of vertices in a complex network (i.e., the probability of a third edge within a set of three vertices given that the two other edges are already known to exist).
- (ii) *Global clustering coefficient*  $\mathcal{C}$  [29], which gives the arithmetic mean of the local clustering coefficient  $C_v$  taken over all vertices  $v$ .  $\mathcal{C}$  is often called the Watts-Strogatz clustering coefficient, which is closely related to  $\mathcal{T}$  but gives more weight to poorly connected vertices [30]. Note that  $\mathcal{T}$  is sometimes referred to as the Barrat-Weigt clustering coefficient. Though  $\mathcal{C}$  and  $\mathcal{T}$  are closely related, in order to avoid confusion, in this work we prefer to discuss both measures separately.
- (iii) *Average path length*  $\mathcal{L}$ , which quantifies the average geodesic distance between all pairs of vertices.
- (iv) *Assortativity coefficient*  $\mathcal{R}$  [31], which characterizes the similarity of the connectivity at both ends of all edges in the network (i.e., the correlation coefficient between the degrees of all pairs of connected vertices).

In many cases, the edge density  $\rho$  (simply representing the present fraction of possible links of the graph) helps to understand the properties of the above global network measures as has been observed in [16].

## 3. Re-sampling algorithm for time series

Recently, an improved algorithm to study the scaling properties of VGs for long-term correlated stochastic processes based on re-sampled time series has been proposed, which allowed a better estimation of the characteristic fractal scaling exponent [23]. The key idea of the algorithm relies on the concept that each pattern in a fractal time series is repeated frequently over different scales [23]. The multiple scales can be captured if proper delays  $\tau$  are continuously introduced to re-sample the original time series. More specifically, considering a scalar time series  $\mathbf{x} = [x_1, x_2, \dots, x_i, \dots, x_N]$  of  $N$  sample times as described above, the proposed re-sampling algorithm consists of the following steps:

- (a) Let initially  $\tau = 1$ , and  $\tau \in \mathbb{Z}$ .
- (b) Re-sample  $\mathbf{x}$  every  $\tau$  steps, which yields new sequences as

$$\mathbf{x}_m^\tau = [x_m, x_{m+\tau}, x_{m+2\tau}, \dots, x_{m+\lfloor \frac{N-m}{\tau} \rfloor \tau}], \quad (m = 1, 2, \dots, \tau), \quad (4)$$

where  $\lfloor \cdot \rfloor$  denotes the lower integer value and  $\tau$  determines the delay between successive points in the sequence  $\mathbf{x}_m^\tau$ . Note that the original time series  $\mathbf{x}$  is recovered when  $\tau = m = 1$ .

- (c) Construct VG and HVG for each sequence  $\mathbf{x}_m^\tau$  ( $m = 1, 2, \dots, \tau$ ). Afterwards, compute all network measures for each segment and the ensemble average over all  $m$  segments.
- (d) Increase  $\tau = \tau + 1$  and repeat steps (b) to (c). The algorithm stops when  $\tau = \tau_{max}$ , for which the network measures remain roughly constant. In the particular case of fractal time series, the double logarithmic plots of  $p(k)$  are expected to show similar scaling regimes where roughly the same power law exponents are estimated for different  $\tau$ .

One of the benefits of re-sampling is that the estimation of the fractal scaling exponent of a time series at multiple scales is more robust against noise, since noise may manifest at one scale but may not be significant at other scales. There is an algorithmic parameter  $\tau$  which should be chosen properly. Put differently, we need to know when we should terminate the computation loop of the algorithm. The original idea of choosing  $\tau_{max}$  is based on the power-law exponents of  $p(k) \sim k^{-\gamma}$  that are computed from the networks. In particular, values of  $\gamma$  are expected to converge if  $\tau \geq \tau_{max}$  [23].

However, it remains largely unclear whether this re-sampling algorithm can be applied to also estimate the parameter  $\lambda$  of exponential scaling laws for stochastic processes. Varying the parameter settings of the AR processes, we will show that network measures strongly depend on the corresponding ACFs. Furthermore, for AR processes, we show that the decorrelation time (which can be expressed as  $\tau_{1/e}$  or  $\tau_{0.1}$ , i.e., time lags after which the estimated ACF has decayed to  $1/e$  or  $0.1$ ) of a time series often yields a good choice of  $\tau_{max}$ .

## 4. Results

In this section, we first demonstrate the effects of the correlation length on the degree distributions, and then study the influence of re-sampling delays on the network measures.

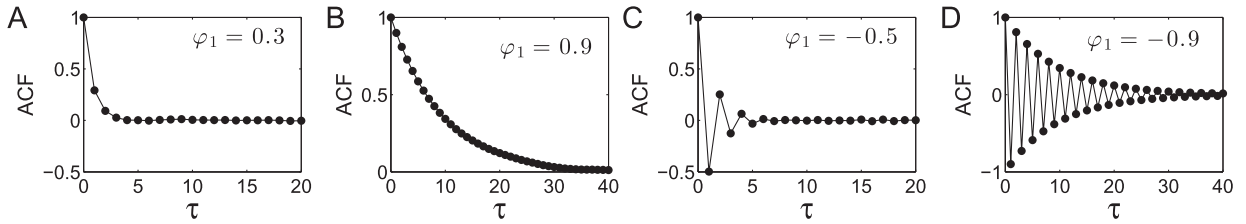


**Fig. 1.** ACFs of AR(1) processes. (A)  $\varphi_1 = 0.3$ . (B)  $\varphi_1 = 0.9$ . (C)  $\varphi_1 = -0.5$ . and (D)  $\varphi_1 = -0.9$ . The correlation length is longer if  $\varphi_1 = 0.9$  than for  $\varphi_1 = 0.3$  as shown by the slow decay of ACF. When  $\varphi_1$  is negative, the ACF alternates around zero and decays to zero more quickly for  $\varphi_1 = -0.5$  (C) than for the case of  $\varphi_1 = -0.9$  (D).

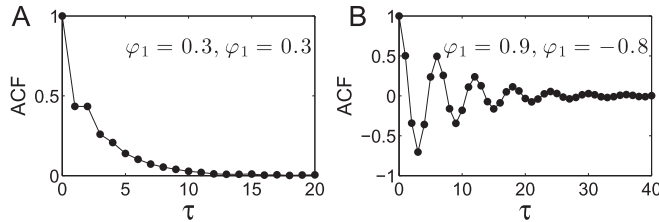


**Fig. 2.** ACFs of AR(2) processes. (A)  $\varphi_1 = 0.3$  and  $\varphi_2 = 0.3$ , and (B)  $\varphi_1 = 0.9$  and  $\varphi_2 = -0.8$ .

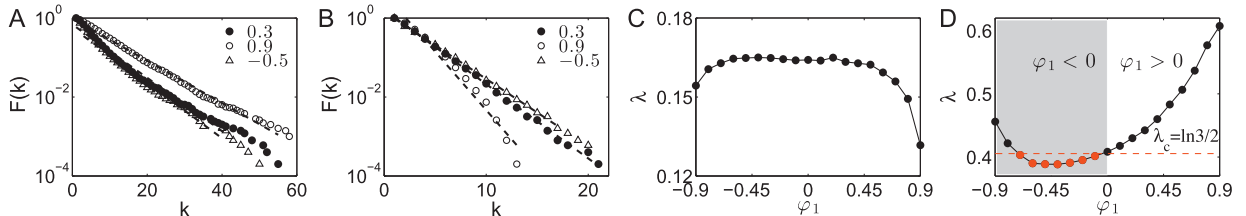


**Fig. 3.** (color online) (A, B) Estimates of  $\lambda$  for approximately exponential degree distributions of AR(1) process. (C, D)  $\lambda$  versus  $\varphi_1$ . (A, C) VG, and (B, D) HVG. When  $\varphi_1 > 0$ ,  $\lambda$  has a decreasing trend in the VG, while in the HVG,  $\lambda$  rises when the correlation length increases. Each dot in panels C and D represents an average over 50 independent random realizations of 5000 data points. In (D),  $\lambda$  values smaller than  $\ln 3/2$  are highlighted by red color. (For interpretation of the references to colour in this figure legend, the reader is referred to the web version of this article.)

#### 4.1. Autocorrelation functions of AR processes

Estimating the ACF of a stationary time series at lag  $\tau$  is straightforward as long as  $\tau$  is small compared to the total length of the time series,  $N$ . The ACF of an AR process can be estimated as the ensemble average of the ACF evaluated for many realizations (in this work, we consider 50 realizations). For stationary stochastic processes, the functional form and rate of decay of the ACF depends on the specific properties of the process [24]. Specifically,

- (a) AR(1) processes have only one degree of freedom, such that no oscillation can arise at longer time-scales. In Fig. 1, we show the ACFs of AR(1) processes for four different parameters:  $\varphi_1 = 0.3$ ,  $\varphi_1 = 0.9$ ,  $\varphi_1 = -0.5$ , and  $\varphi_1 = -0.9$ . When increasing  $\varphi_1$  from 0.3 to 0.9, the correlation length becomes larger, which is characterized by a slower decay of the ACF (Fig. 1A and B). A negative coefficient  $\varphi_1$  results in the ACF alternating around zero (Fig. 1C). Again, a smaller negative  $\varphi_1$  leads to a slower decay to zero (Fig. 1D).
- (b) AR(2) processes have two degrees of freedom and can oscillate depending on the choice of the parameters  $\varphi_1$  and  $\varphi_2$ . For instance, when  $\varphi_1 = 0.3$  and  $\varphi_2 = 0.3$ , the process has a behavior comparable to that of an AR(1) process with slow decay of correlations (shown in Fig. 2A). However, when  $\varphi_1 = 0.9$  and  $\varphi_2 = -0.8$ , the AR(2) process shows a quasi-periodic behavior as shown in Fig. 2B.

#### 4.2. Effects of the correlation length on degree distributions

Let us start with the case of  $\varphi_1 > 0$  in the AR(1) model. We find that  $p(k)$  approximately follows an exponential distribution. To illustrate this finding, the cumulative degree distributions  $F(k) = 1 - \int_0^k p(k)dk \sim e^{-\lambda k}$  for  $\varphi_1 = 0.3$ , 0.9 and  $-0.5$  are shown in Fig. 3A and B, where clear scaling regimes are present in the semi-logarithmic plots. Furthermore, we find that the exponents  $\lambda$  estimated for VGs are smaller than those are estimated for HVGs. When increasing  $\varphi_1$ , in the VG, the exponent  $\lambda$  shows a monotonically decreasing trend (Fig. 3C). In contrast, the value  $\lambda$  for the HVG is increased (Fig. 3D).

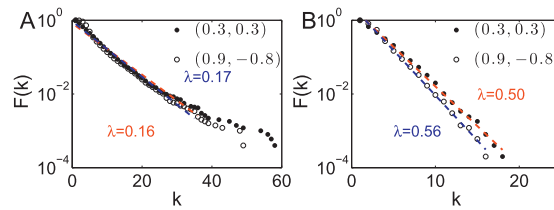


**Fig. 4.** Estimates of  $\lambda$  of exponential degree distribution functions of AR(2) processes. The length of the time series is 5000 points. (A) VG, (B) HVG, where  $\lambda > \lambda_c = \ln 3/2$  for both  $(\varphi_1, \varphi_2) = (0.3, 0.3)$  and  $(\varphi_1, \varphi_2) = (0.9, -0.8)$ .

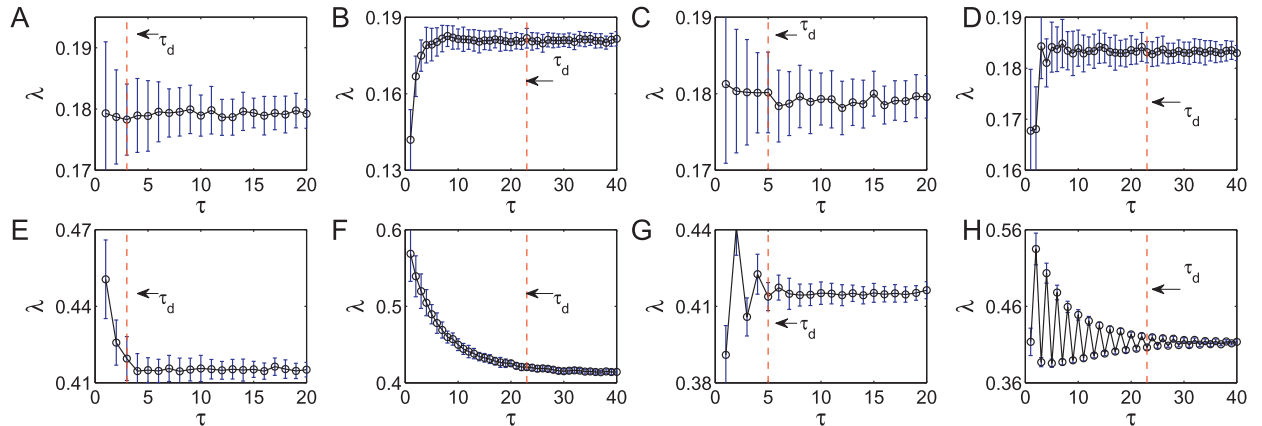


**Fig. 5.** Estimates of the scaling parameter  $\lambda$  versus re-sampling delay  $\tau$  for AR(1) processes (error bars indicating standard deviations obtained over 50 independent random realizations). (A, E)  $\varphi_1 = 0.3$ , (B, F)  $\varphi_1 = 0.9$ , (C, G)  $\varphi_1 = -0.5$ , and (D, H)  $\varphi_1 = -0.9$ . The results have been obtained for VG (A–D), and HVG (E–H), respectively. The vertical dashed lines indicate the positions of  $\tau_{0.1}$ , where the ACFs decay to 0.1.

The result of Fig. 3D confirms the hypothesis stated in [18] that all  $\lambda$  should be larger than  $\lambda_c = \ln(3/2)$  as the correlation length is increased in the case of positively correlated increments.

In turn, when  $\varphi_1 < 0$ , we observe some peculiar results that seem to contradict the hypothesis stated in [18]. According to this hypothesis,  $\lambda$  should be larger than  $\lambda_c$  ( $\lambda > \lambda_c$ ) in stochastic processes in contrast to  $\lambda < \lambda_c$  for chaotic maps. The results of Fig. 3D do not support this claim when  $\varphi_1$  is negative in the AR(1) model. Instead, we find a region where the slope of the exponential degree distribution is smaller than  $\ln(3/2)$  (as highlighted in Fig. 3D). This suggests that the critical value of  $\ln(3/2)$  should not be understood as a general law of separating correlated stochastic from chaotic processes, which requires further investigation.

Fig. 4 shows the estimation of  $\lambda$  for two examples of AR(2) models. In contrast to the AR(1) processes in Fig. 3, the values of  $\lambda$  are larger than  $\lambda_c$  consistent with the argument of [18] as the correlation length is increased. In the case of varying parameters  $\varphi_1, \varphi_2$  of the AR(2) model, we expect to have similar results as for the AR(1) case since  $\lambda$  depends on the sign of correlations between the increments of the underlying processes.

#### 4.3. Effects of re-sampling delays on the network characteristics

First, we note that the length of a time series might affect the network statistics of (H)VGs. According to the original idea of the re-sampling algorithm, we generate a time series of length  $N$ , say  $N = 1000$  points. The network size of the original time series is  $N = 1000$  when  $\tau = 1$ . When  $\tau$  is increased to 10, there are 10 segmented sequences, each having 100 data points, where the network size of each sequence is  $N = 100$ . Clearly, the network sizes are systematically reduced when increasing  $\tau$ . In turn, the recommended strategy is to guarantee that each network from different  $\tau$  has the same size, which is often required to avoid sample size effects when comparing network measures. A simple solution in the case of stationary processes could be the following: we generate a much longer time series of length  $L = N \times \tau$ . The first  $N = 1000$  points are taken for a sampling delay  $\tau = 1$ . According to the re-sampling algorithm, for any  $\tau \geq 2$  we re-sample from  $L$  time points in such a way that each re-sampled sequence has the same length of  $N = 1000$  points as  $\tau = 1$ .

The results are summarized in the following:

(a) Estimated scaling parameter of exponential degree distributions (Figs. 5 and 6).

The estimates of the exponential scaling parameter  $\lambda$  show non-trivial dependencies on the behavior of ACFs. More specifically, for positive values of  $\varphi_1$  of AR(1) models, the convergence of  $\lambda$  to some constant values is significantly delayed when  $\varphi_1$  is increased from 0.3 to 0.9 (shown in Fig. 5A and B (VG), D and E (HVG)). For negative  $\varphi_1$  values,

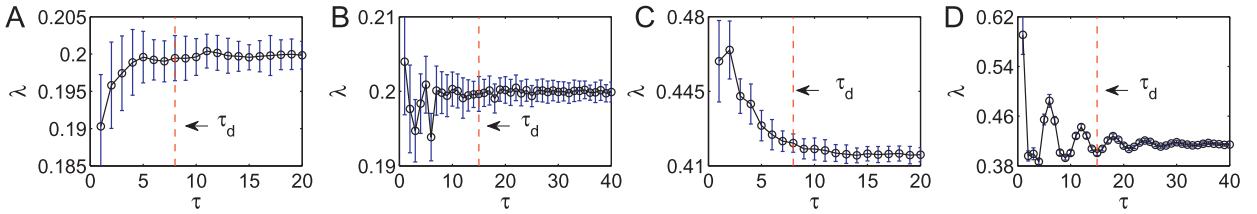


**Fig. 6.** Estimated scaling parameters  $\lambda$  versus re-sampling delay  $\tau$  for AR(2) processes (error bars indicating the standard deviations obtained over 50 independent random realizations). (A, C)  $\varphi_1 = 0.3$  and  $\varphi_2 = 0.3$ , and (B, D)  $\varphi_1 = 0.9$  and  $\varphi_2 = -0.8$ . Results have been obtained from VG (A, B), and HVG (C, D), respectively. The vertical dashed lines indicate the positions of  $\tau_{0.1}$ , where ACFs decay to 0.1.

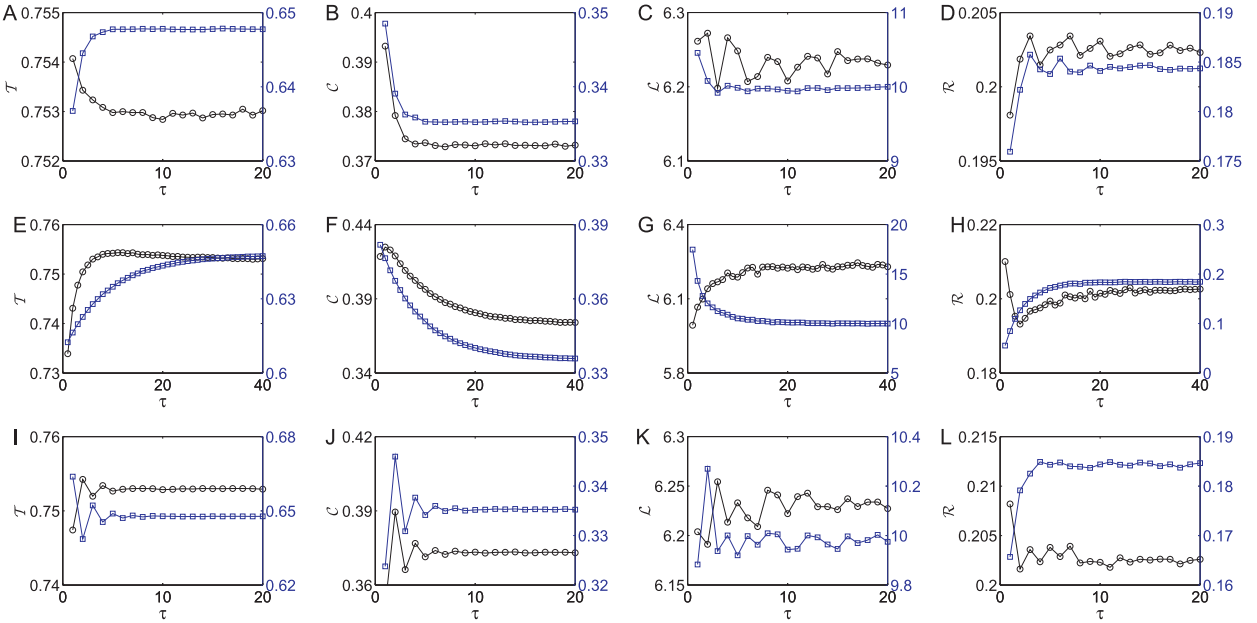


**Fig. 7.** Network properties versus re-sampling time delay  $\tau$  in AR(1) processes. Positively correlated increments (A–D)  $\varphi_1 = 0.3$ , (E–H)  $\varphi_1 = 0.9$ , and negatively correlated increments (I–L)  $\varphi_1 = -0.5$ . (A, E, I) transitivity  $\mathcal{T}$ , (B, F, J) clustering coefficient  $\mathcal{C}$ , (C, G, K) average shortest path length  $\mathcal{L}$ , and (D, H, L) assortativity  $\mathcal{R}$ . y-axes on the left side of each panel are for VGs ( $\circ$ ), and results of HVGs ( $\square$ ) are aligned to the right y-axes.

the convergence becomes faster if  $\varphi_1 = -0.5$  (Fig. 5C) than that of the case of  $-0.9$  (Fig. 5D). Slow decays have also been found in AR(2) models with positive values of both  $\varphi_1$  and  $\varphi_2$  (Fig. 6A and C). However, oscillations appear when  $\varphi_2 = -0.8$  in the AR(2) process (Fig. 6B and D). Taken together, in the AR(2) process with negative parameter  $\varphi_2$ , a stable value of  $\lambda$  is often not expected if the re-sampling delay  $\tau$  is small.

(b) Global measures:  $\mathcal{T}$ ,  $\mathcal{C}$ ,  $\mathcal{L}$ , and  $\mathcal{R}$  (Figs. 7 and 8).

All considered global network measures show similar variation patterns as the ACFs do themselves. For instance, the effects due to increasing correlation lengths are clearly captured by all network measures, showing slower convergence to constant values when  $\varphi_1$  is increased from 0.3 to 0.9 in the AR(1) model (cf. each panel of Fig. 7(A–D) to (E–H)). When  $\varphi_1 < 0$ , the network measures display oscillatory behavior but quickly approach stable values if  $\varphi_1 = -0.5$  (Fig. 7(I–L)). The corresponding results for AR(2) models with positive parameters  $\varphi_1$  and  $\varphi_2$  are shown in Fig. 8(A–D). The damped oscillation patterns of AR(2) with negative  $\varphi_2$  are well captured by all network measures (Fig. 8(E–H)). Consistent results have been obtained for VGs and HVGs. Note that in Figs. 7 and 8, results for VGs are aligned to the left y-axes, while the right y-axes are for the results of HVGs.

(c) Decorrelation time  $\tau_d$  as a proxy for  $\tau_{max}$ .

In general, the hypothetical monotonical convergence of all network measures with increasing re-sampling delay is not found in AR processes. In nonlinear time series analysis, the decorrelation time  $\tau_d$  is often suggested for attractor reconstruction from scalar time series [32]. Empirically,  $\tau_d$  is expressed as  $\tau_{1/e}$  or  $\tau_{0.1}$ , i.e., the time lags after which the estimated ACF has decayed to  $1/e$  or 0.1, respectively, which often yield good estimates of the decorrelation time. We find that the decorrelation time  $\tau_d$  as an upper limit for the re-sampling delay commonly leads to a reliable estimation of  $\lambda$ . More specifically, the variances  $\sigma_\lambda$  of the estimated values of  $\lambda$  based on 50 independent random realizations are significantly smaller when  $\tau_{0.1}$  is used for the segmentation, in comparison to the case of  $\tau_d = 1$  in

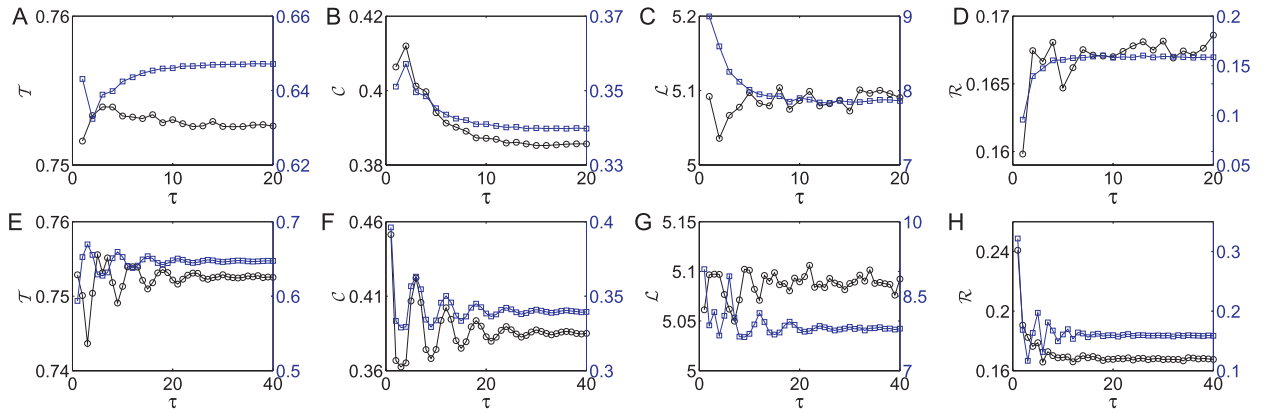


**Fig. 8.** Network properties versus re-sampling time delay  $\tau$  in AR(2) processes. The correlation lengths are captured in (A–D)  $\varphi_1 = \varphi_2 = 0.3$ , and oscillation patterns appear in (E–H)  $\varphi_1 = 0.9$ , and  $\varphi_2 = -0.8$ . (A, E) transitivity  $\mathcal{T}$ , (B, F) clustering coefficient  $\mathcal{C}$ , (C, G) average shortest path length  $\mathcal{L}$ , and (D, H) assortativity  $\mathcal{R}$ .  $y$ -axes on the left side of each panel are for VGs ( $\circ$ ), and results of HVGs ( $\square$ ) are aligned to the right  $y$ -axes.

the original VG analysis (see error-bars in Figs. 5 and 6). Based on these observations, we conjecture that values of  $\lambda$  converge to the case of white noise, i.e., uncorrelated stochastic processes, when  $\tau > \tau_{max} = \tau_d$ . Similar convergence of global network measures to the values for white noise when  $\tau > \tau_d$  is shown in Figs. 7 and 8.

## 5. Conclusions

In summary, we have performed a systematic (H)VG analysis for time series generated by auto-regressive (AR) processes. We have found the approximate presence of exponential degree distributions (fully determined by a single exponential scaling parameter  $\lambda$ ) for AR models. Our results for AR(1) models with a positive parameter  $\varphi_1$  are in favor of the hypothesis that all  $\lambda > \lambda_c = \ln 3/2$  when the correlation length is increased in short-term correlated stochastic processes. In turn, we have observed that a pronounced interval of negative  $\varphi_1$  where  $\lambda < \lambda_c$ . This result suggests that the previously considered critical value of  $\ln(3/2)$  should not be interpreted as a general law of separating correlated stochastic from chaotic processes. Further understanding of this finding requires both theoretical and numerical investigation.

We have furthermore checked the applicability of the re-sampling algorithm to AR processes. The properties of (H)VGs show non-trivial dependence on the re-sampling delay  $\tau$ . More specifically, network measures show (i) slow decays when the correlation length is increased, and (ii) oscillations when the second coefficient  $\varphi_2$  of an AR(2) process becomes negative. Furthermore, we have proposed the decorrelation time  $\tau_d$  as an educated choice of the maximal time delay  $\tau_{max}$  in the re-sampling algorithm. This shares the same spirit as the fact that the time delay  $\tau$  is often used for time-delay embedding when performing nonlinear time series analysis in phase space [32]. Our detailed comparison demonstrates that network measures often converge to different values between the original VGs and HVGs, when increasing the time delay  $\tau$ . Note that the delay  $\tau$  introduced in the re-sampling algorithm is different from the case where time-shifted series are used to test irreversibility of non-stationary processes [16,33–35].

Although it has been shown that the HVG condition yields network edges that are a subset of the original visibility criterion [18], the resulting networks' structural properties might be quite different. Further network measures (e.g., betweenness) have not been further discussed here in the present work. It is worth pointing out that, to this end, proper interpretations of the global network measures in terms of the dynamical properties of the underlying dynamical system largely remain unclear.

Studying time series from complex network perspectives has attained considerable interest and has led to the development of a plethora of algorithms highlighting different aspects of the complex dynamics encoded in time series data. In this work, we have focused on stationary processes, however, many real-world processes are non-stationary. For instance, climate or hydrological data often show seasonal variations. Non-stationary behaviors can be expressed in terms of trends, cycles, random walks, or combinations of them, especially when self-similarity is involved. One classical example is fractional Brownian motion (fBm), which has long-range temporal correlations as its defining property [36]. It has been argued that self-similarity properties of fBm can be successfully captured by VG analysis [18,21,22]. We note that fitting a power-law to empirical data and assessing the accuracy of the scaling exponent  $\gamma$  is a complicated problem [26]. Concerning the re-sampling algorithm on fBm, most likely one obtains only some properties that are specific for one realization of the process of a particular length. This is because the autocorrelation of fBm processes shows arbitrarily long time-scales due to the self-similar nature of the process. In other words, all or almost all values are correlated with one another at very long lags in time. This makes finding a suitable value of  $\tau$  a challenging task, which has been demonstrated in detail in [37].

## Acknowledgements

Parts of this work have been financially supported by the National Natural Science Foundation of China (Grant Nos. 11305062, 11405059, 61473203). We acknowledge valuable comments by Reik V. Donner.

## References

- [1] Zhang J, Small M. Complex network from pseudoperiodic time series: Topology versus dynamics. *Phys Rev Lett* 2006;96(23):238701. doi:[10.1103/PhysRevLett.96.238701](https://doi.org/10.1103/PhysRevLett.96.238701).
- [2] Xu X, Zhang J, Small M. Superfamily phenomena and motifs of networks induced from time series. *Proc Natl Acad Sci USA* 2008;105(50):19601–5. doi:[10.1073/pnas.0806082105](https://doi.org/10.1073/pnas.0806082105).
- [3] Lacasa L, Luque B, Ballesteros F, Luque J, Nuno JC. From time series to complex networks: the visibility graph. *Proc Natl Acad Sci USA* 2008;105(13):4972–5. doi:[10.1073/pnas.0709247105](https://doi.org/10.1073/pnas.0709247105).
- [4] Marwan N, Donges JF, Zou Y, Donner RV, Kurths J. Complex network approach for recurrence analysis of time series. *Phys Lett A* 2009;373(46):4246–54. doi:[10.1016/j.physleta.2009.09.042](https://doi.org/10.1016/j.physleta.2009.09.042).
- [5] Donner RV, Zou Y, Donges JF, Marwan N, Kurths J. Recurrence networks – a novel paradigm for nonlinear time series analysis. *New J Phys* 2010;12(3):033025. doi:[10.1088/1367-2630/12/3/033025](https://doi.org/10.1088/1367-2630/12/3/033025).
- [6] Donner RV, Small M, Donges JF, Marwan N, Zou Y, Xiang R, et al. Recurrence-based time series analysis by means of complex network methods. *Int J Bifurcat Chaos* 2011a;21(4):1019–46. doi:[10.1142/S0218127411029021](https://doi.org/10.1142/S0218127411029021).
- [7] Donges JF, Donner RV, Trauth MH, Marwan N, Schellnhuber HJ, Kurths J. Nonlinear detection of paleoclimate-variability transitions possibly related to human evolution. *Proc Natl Acad Sci USA* 2011;108:20422–7. doi:[10.1073/pnas.1117052108](https://doi.org/10.1073/pnas.1117052108).
- [8] Zou Y, Donner RV, Wickramasinghe M, Kiss IZ, Small M, Kurths J. Phase coherence and attractor geometry of chaotic electrochemical oscillators. *Chaos* 2012;22(3):033130. doi:[10.1063/1.4747707](https://doi.org/10.1063/1.4747707).
- [9] Gao Z, Zhang X, Jin N, Donner RV, Marwan N, Kurths J. Recurrence networks from multivariate signals for uncovering dynamic transitions of horizontal oil-water stratified flows. *Europhys Lett* 2013;103(5):50004. doi:[10.1209/0295-5075/103/50004](https://doi.org/10.1209/0295-5075/103/50004).
- [10] Donner RV, Small M, Donges JF, Marwan N, Zou Y, Xiang R, et al. Recurrence-based time series analysis by means of complex network methods. *Int J Bifurcat Chaos* 2011b;21(4):1019–46. doi:[10.1142/S0218127411029021](https://doi.org/10.1142/S0218127411029021).
- [11] Elsner JB, Jagger TH, Fogarty EA. Visibility network of united states hurricanes. *Geophys Res Lett* 2009;36(16):L16702. doi:[10.1029/2009GL039129](https://doi.org/10.1029/2009GL039129).
- [12] Yang Y, Wang J, Yang H, Mang J. Visibility graph approach to exchange rate series. *Physica A* 2009;388(20):4431–7. doi:[10.1016/j.physa.2009.07.016](https://doi.org/10.1016/j.physa.2009.07.016).
- [13] Liu C, Zhou W-X, Yuan W-K. Statistical properties of visibility graph of energy dissipation rates in three-dimensional fully developed turbulence. *Physica A* 2010;389(13):2675–81. doi:[10.1016/j.physa.2010.02.043](https://doi.org/10.1016/j.physa.2010.02.043).
- [14] Gao Z, Du M, Hu L, Zhou T, Jin N. Visibility graphs from experimental three-phase flow for characterizing dynamic flow behavior. *Int J Mod Phys C* 2012;23(10):1250069. doi:[10.1142/S0129183112500696](https://doi.org/10.1142/S0129183112500696).
- [15] Zou Y, Small M, Liu Z, Kurths J. Complex network approach to characterize the statistical features of the sunspot series. *New J Phys* 2014;16(1):013051. doi:[10.1088/1367-2630/16/1/013051](https://doi.org/10.1088/1367-2630/16/1/013051).
- [16] Zou Y, Donner R, Marwan N, Small M, Kurths J. Long-term changes in the north-south asymmetry of solar activity: a nonlinear dynamics characterization using visibility graphs. *Nonlin Proc Geophys* 2014b;21(6):1113–26. doi:[10.5194/npg-21-1113-2014](https://doi.org/10.5194/npg-21-1113-2014).
- [17] Luque B, Lacasa L, Ballesteros F, Luque J. Horizontal visibility graphs: exact results for random time series. *Phys Rev E* 2009;80(4):046103. doi:[10.1103/PhysRevE.80.046103](https://doi.org/10.1103/PhysRevE.80.046103).
- [18] Lacasa L, Toral R. Description of stochastic and chaotic series using visibility graphs. *Phys Rev E* 2010;82:036120. doi:[10.1103/PhysRevE.82.036120](https://doi.org/10.1103/PhysRevE.82.036120).
- [19] Lacasa L. On the degree distribution of horizontal visibility graphs associated with markov processes and dynamical systems: diagrammatic and variational approaches. *Nonlinearity* 2014;27(9):2063. doi:[10.1088/0951-7715/27/9/2063](https://doi.org/10.1088/0951-7715/27/9/2063).
- [20] Ravetti MG, Carpi LC, Goniálves BA, Frery AC, Rosso OA. Distinguishing noise from chaos: objective versus subjective criteria using horizontal visibility graph. *PLoS ONE* 2014;9(9):E108004. doi:[10.1371/journal.pone.0108004](https://doi.org/10.1371/journal.pone.0108004).
- [21] Lacasa L, Luque B, Luque J, Nuno JC. The visibility graph: a new method for estimating the hurst exponent of fractional brownian motion. *Europhys Lett* 2009;86(3):30001. doi:[10.1209/0295-5075/86/30001](https://doi.org/10.1209/0295-5075/86/30001).
- [22] Ni X-H, Jiang Z-Q, Zhou W-X. Degree distributions of the visibility graphs mapped from fractional brownian motions and multifractal random walks. *Phys Lett A* 2009;373(42):3822–6. doi:[10.1016/j.physleta.2009.08.041](https://doi.org/10.1016/j.physleta.2009.08.041).
- [23] Ahmadlou M, Adeli H, Adeli A. Improved visibility graph fractality with application for the diagnosis of autism spectrum disorder. *Physica A* 2012;391(20):4720–6. doi:[10.1016/j.physa.2012.04.025](https://doi.org/10.1016/j.physa.2012.04.025).
- [24] Witt A, Malamud B. Quantification of long-range persistence in geophysical time series: Conventional and benchmark-based improvement techniques. *Surv Geophys* 2013;34(5):541–651. doi:[10.1007/s10712-012-9217-8](https://doi.org/10.1007/s10712-012-9217-8).
- [25] Beran J. *Statistics for long-memory processes*. Boca Raton: Chapman and Hall/CRC; 1994.
- [26] Clauset A, Shalizi CR, Newman MEJ. Power-law distributions in empirical data. *SIAM Rev* 2009;51(4):661–703. doi:[10.1137/070710111](https://doi.org/10.1137/070710111).
- [27] Newman MEJ. Scientific collaboration networks. i. network construction and fundamental results. *Phys Rev E* 2001;64(1):016131. doi:[10.1103/PhysRevE.64.016131](https://doi.org/10.1103/PhysRevE.64.016131).
- [28] Barrat A, Weigt M. On the properties of small-world network models. *Eur Phys J B* 2000;13:547–60. doi:[10.1007/s100510050067](https://doi.org/10.1007/s100510050067).
- [29] Watts DJ, Strogatz SH. Collective dynamics of “small-world” networks. *Nature* 1998;393(6684):440–2. doi:[10.1038/30918](https://doi.org/10.1038/30918).
- [30] Donner RV, Heitzig J, Donges JF, Zou Y, Marwan N, Kurths J. The geometry of chaotic dynamics – a complex network perspective. *Eur Phys J B* 2011c;84(4):653–72. doi:[10.1140/epjb/e2011-10899-1](https://doi.org/10.1140/epjb/e2011-10899-1).
- [31] Newman MEJ. Assortative mixing in networks. *Phys Rev Lett* 2002;89(20):208701. doi:[10.1103/PhysRevLett.89.208701](https://doi.org/10.1103/PhysRevLett.89.208701).
- [32] Kantz H, Schreiber T. *Nonlinear time series analysis*. 2nd ed. Cambridge: Cambridge University Press; 2004.
- [33] Lacasa L, Nuñez A, Roldán E, Parrondo JMR, Luque B. Time series irreversibility: a visibility graph approach. *Eur Phys J B* 2012;85:217. doi:[10.1040/epjb/e2012-20809-8](https://doi.org/10.1040/epjb/e2012-20809-8).
- [34] Donges JF, Donner RV, Kurths J. Testing time series irreversibility using complex network methods. *Europhys Lett* 2013;102(1):10004. doi:[10.1209/0295-5075/102/10004](https://doi.org/10.1209/0295-5075/102/10004).
- [35] Lacasa L, Flanagan R. Time reversibility from visibility graphs of nonstationary processes. *Phys Rev E* 2015;92:022817. doi:[10.1103/PhysRevE.92.022817](https://doi.org/10.1103/PhysRevE.92.022817).
- [36] Mandelbrot B, Ness JV. Fractional brownian motions, fractional noises and applications. *SIAM Rev* 1968;10(4):422–37. doi:[10.1137/1010093](https://doi.org/10.1137/1010093).
- [37] Zou Y, Donner RV, Kurths J. Analyzing long-term correlated stochastic processes by means of recurrence networks: potentials and pitfalls. *Phys Rev E* 2015;91:022926. doi:[10.1103/PhysRevE.91.022926](https://doi.org/10.1103/PhysRevE.91.022926).